metals

MDPI

Article

Microstructural Evolution as a Function of Increasing Aluminum Content in Novel Lightweight Cast Irons

Alejandro Obregon [1,*], Jon Mikel Sanchez [1,*], David Eguizabal [1,*], Jose Carlos Garcia [1], Gurutze Arruebarrena [2], Iñaki Hurtado [2], Ion Quintana [3] and Patxi Rodriguez [3]

[1] TECNALIA, Basque Research and Technology Alliance (BRTA), 48160 Derio, Spain; josecarlos.garcia@tecnalia.com
[2] Faculty of Engineering, Mondragon Unibertsitatea, 20500 Arrasate-Mondragon, Spain; garruebarrena@mondragon.edu (G.A.); ihurtado@mondragon.edu (I.H.)
[3] EDERTEK Technology Centre, Fagor Ederlan Group, 20500 Arrasate-Mondragon, Spain; i.quintana@edertek.es (I.Q.); p.rodriguez@edertek.es (P.R.)
* Correspondence: alejandro.obregon@tecnalia.com (A.O.); jonmikel.sanchez@tecnalia.com (J.M.S.); david.eguizabal@tecnalia.com (D.E.)

Abstract: In the context of the development of new lightweight materials, Al-alloyed cast irons have a great potential for reducing the weight of the different part of the vehicles in the transport industry. The correlation of the amount of Al and its effect in the microstructure of cast irons is not completely well established as it is affected by many factors such as chemical composition, cooling rate, etc. In this work, four novel lightweight cast irons were developed with different amounts of Al (from 0 wt. % to 15 wt. %). The alloys were manufactured by an easily scalable and affordable gravity casting process in an induction furnace, and casted in a resin-bonded sand mold. The microstructural evolution as a function of increasing Al content by different microstructural characterization techniques was studied. The hardness of the cast irons was measured by the Vickers indentation test and correlated with the previously characterized microstructures. In general, the microstructural evolution shows that the perlite content decrease with the increment of wt. % of Al. The opposite occurs with the ferrite content. In the case of graphite, a slight increment occurs with 2 wt. % of Al, but a great decrease occurs until 15 wt. % of Al. The addition of Al promotes the stabilization of ferrite in the studied alloys. The hardness obtained varied from 235 HV and 363 HV in function of the Al content. The addition of Al increases the hardness of the studied cast irons, but not gradually. The alloy with the highest hardness is the alloy containing 7 wt. % Al, which is correlated with the formation of kappa-carbides and finer perlite.

Keywords: cast iron; microstructure; casting; modelling; light-weighting; hardness

Citation: Obregon, A.; Sanchez, J.M.; Eguizabal, D.; Garcia, J.C.; Arruebarrena, G.; Hurtado, I.; Quintana, I.; Rodriguez, P. Microstructural Evolution as a Function of Increasing Aluminum Content in Novel Lightweight Cast Irons. *Metals* **2021**, *11*, 1646. https://doi.org/10.3390/met11101646

Academic Editor: Cristiano Fragassa

Received: 15 September 2021
Accepted: 14 October 2021
Published: 18 October 2021

Publisher's Note: MDPI stays neutral with regard to jurisdictional claims in published maps and institutional affiliations.

Copyright: © 2021 by the authors. Licensee MDPI, Basel, Switzerland. This article is an open access article distributed under the terms and conditions of the Creative Commons Attribution (CC BY) license (https://creativecommons.org/licenses/by/4.0/).

1. Introduction

Weight reduction has become an important element to reduce greenhouse gas emissions in the transport industry. A great deal of effort is being made in the development of novel materials with improved mechanical and/or physical properties, with light weight as the main goal. The transport industry depends on the development of new lightweight materials to optimize the fuel consumption of the next generation of vehicles. Therefore, with the goal of complying with global vehicle emissions regulations, the research focus is on the development of new materials to replace traditional alloys for reducing energy consumption and, thereby, gas emissions (NOx, CO_2, etc.). In addition, new materials should not compromise structural properties, or contribute to significant cost increases. In this way, novel materials such as complex concentrated alloys, medium/high entropy alloys, aluminum-based hybrid composites, etc. has been developed in the last years [1–5].

As steels are alloys mainly formed by one of the most abundant elements in the Earth's crust, and the most used engineering alloys; the development of new lightweight steels have become a hot topic in materials science. Hence, novel lightweight steels with improved specific strength and/or ductility have been developed, by alloying light elements such as Al or Si [6–12]. On the other hand, few investigations have been carried out to develop novel lightweight cast irons. To date, the strategy most employed is to develop high-strength lightweight cast irons by alloying a large amount of Al. Approximately, the density of traditional cast irons can be decreased to a value below 7 g/cm^3 by alloying ~5 wt. % Al and near 6 g/cm^3 by alloying ~15 wt. % Al [13,14]. In addition, cast irons meet one of the previously mentioned requirements for light weighting at a reasonable cost. Depending on its concentration, the introduction of Al in cast iron has a significant effect on the microstructure of the alloy, as well as on the mechanical properties [15].

Some research has been done to correlate the amount of Al and its effect in the microstructure. The correlation of the amount of Al and its effect in the microstructure of cast irons is not completely well established as it is affected by many factors such as chemical composition, cooling rate, inoculation and melting treatments [16,17]. For example, Ibrahim et al. [18] concluded that increasing Al content within a certain range up to 4 wt. % facilitated the cast iron graphitization, but its further increase suppressed the graphite precipitation and promoted the formation of carbides. On the other hand, Gumienny et al. [19] concluded that Al with a concentration of up to 2.4 wt.% in compacted graphite iron exhibits graphitizing properties, above this concentration it is a carbide-forming element. In the same research, it was also pointed out that with an Al content higher than 8 wt. % the $AlFe_3C_{0.5}$ carbide is precipitated, and that a concentration higher than 3.1 wt. % of Al causes carbide spheroidization in the eutectoid mixture, replacing cementite by κ-carbides (kappa-carbides). Shayesteh-Zeraati et al. [20] studied Al-alloyed ductile cast iron containing 0.48 wt. %, 4.88 wt. % and 6.16 wt. % Al. The results showed that increasing the Al content leads to the decrease of free ferrite and carbides, as well as an increase in the pearlite volume fraction. In the same research, also was reported that increasing the Al content, more intermetallic compounds (Al_6Fe, $AlFe_3C_{0.5}$, Fe_3Al and FeAl) were stabilized.

The complexity of the metallurgy of lightweight cast irons is not only due to the addition of Al, but also to other secondary elements such as Si. For example, Si is well known as an important influencing factor in the solidification of ductile cast irons [21]. As the addition of Al promotes the graphitization of the alloy, Si is employed to avoid metastable iron carbide solidification in gray cast iron [21]. In addition, Kasvayee et al. [22] showed that graphite content, graphite nodule count and ferrite fraction were increased by increasing the Si content, resulting in an increase in yield strength.

Although the aforementioned metallurgical complexity of lightweight cast irons, several benefits have been reported in the mechanical and physical properties, especially in terms of hardness, which is the most studied property. Takamori et al. [23] studied several Al-alloyed cast irons with 3.2 wt. % C, from 1.6 wt. % to 2.4% Si, and from 0 wt. % to 20 wt. % Al. It was concluded that the addition of 12 wt. % of Al improved wear resistance due to the precipitation of carbides but deteriorated the damping capacity. Furthermore, the addition of over 6 wt. % of Al improved the heat resistance, and a content over 20 wt. % produced non-magnetic anticorrosion alloys. The wear resistance also was improved by increasing the Al content in ductile irons, specifically in the alloys containing 2.29 wt. %, 3.02 wt. %, and 3.74 wt. % Al [24]. Ibrahim et al. [18] studied the hardness, oxidation resistance and damping capacity of Al-alloyed (up to 16 wt. % Al) ductile and white cast irons. The hardness was increased up to 500 HV in alloys containing 9 wt. %, 13 wt. % and 14 wt. %. Al, it was attributed to the formation of FeAl, $AlFe_3C$ and Fe_3Al compounds. The oxidation resistance was enhanced by increasing Al content to 5.8 wt. % due to the formation of Al_2O_3. Finally, the damping capacity also was improved in the same alloys, especially in the alloys with 2.6 wt. % and 16.0 wt. %Al. In another work [20], the Fe-3.7C-0.5Al-1.0Si, Fe-3.4C-4.9Al-1.2Si and Fe-3.2C-6.2Al-1.2Si cast irons were studied, obtaining

higher hardness values as a function of increasing Al content, 305 HV, 377 HV and 411 HV respectively. Aguado et al. [21] improved the standard properties of Fe-C–Si grey cast irons, obtaining a strength of 466 MPa and hardness up to 260 HV for an iron with 3.08 wt. % C, 3.15% Al and 0.16 wt. % Si. Recently, the tribological properties of Al-alloyed ductile cast irons were studied, the best wear properties was achieved by the 4 wt. % Al-alloyed nodular cast iron [25]. In the same work, the hardness of the EN-GJS-400–15 grade was augmented in function of increasing the amount of Al, obtaining the highest hardness value in the alloy containing 4 wt. % of Al.

Therefore, the aforementioned properties of the lightweight cast irons make them very interesting alloys for the automotive industry, especially as brake disc material, engine gears, pump housings, etc. Motivated by the above concerns, and because of the great potential that lightweight cast iron to reduce the density and overpass the mechanical properties of traditional cast irons, this study developed four novel Fe-Al-C-Si lightweight gray cast iron alloys. The microstructural evolution of EN-GJL-HB195 grade cast iron alloyed with Al between 0 wt. % and 15 wt. % was studied by different characterization techniques, and the hardness values were obtained for each alloy. It should be mentioned that the alloys were manufactured by easily scalable gravity casting process, and the use of expensive or scarce elements was avoided.

2. Materials and Methods

2.1. Calculation of Equilibrium Phase Diagram

The software Thermo-Calc (v. 2020, Thermo-Calc Software AB, Stockholm, Sweden) [26] in conjunction with the TCFE6 thermodynamic database was used for calculations of the equilibrium phases as a function of temperature.

2.2. Materials Preparation

For the preparation of gray cast irons with different percentages of Al, a 20 kg medium frequency induction furnace VIP-I (Inductotherm Corp., Rancocas, VT, USA) was used. As charge material, 14 kg of low alloying steel scrap was used. Once the charge material was melted, the chemical composition was adjusted to the target composition by using FeSi (75 wt. % Si, 0.073 wt. % C, 0.01 wt. % S, 0.019 wt. % P) and graphite (99 wt. % C). After adjusting, the melt was overheated to ~1500 °C and the elemental composition of the molten bath was analyzed using optical emission spectrometry (OES) before alloying Al, and the results are shown in Table 1.

Table 1. Elemental composition of the molten bath before alloying obtained by optical emission spectrometry (OES).

Fe	C	Si	Mn	Cr	Ni	Mo	Cu	Sn	P	S
Bal.	3.12	2.0	0.63	0.15	0.06	0.01	0.09	0.01	0.02	0.03

After that, pure Al (99 wt. %) was added to obtain the targets compositions with different predetermined amounts of Al (0 wt. %, 2 wt. %, 7 wt. %, and 15 wt. %, referred to as 0-Al, 2-Al, 7-Al and 15-Al, respectively). When the target composition of each alloy was obtained, the alloys were individually casted in a resin-bonded sand mold. Approximately 500 g of each alloy was obtained in a cylindrical (Ø 20 × 50 mm) sample.

2.3. Microstructural and Elemental Characterization.

Before casting, Thermal Analysis (TA) samples were poured into standard QuiK-Cup® sand cups. The data for TA was collected using a high-speed National Instruments Data Acquisition System. The final chemical composition of the four alloys was determined by ICP.

The samples for optical microscopy (OM) and the microhardness test were cut from the bulk samples and prepared according to standard metallographic procedures, by hot

mounting in conductive resin, grinding, and polishing. Graphite distribution type and amount (area %) were defined using image analysis computer tools. Afterward, the samples were etched with Nital 5 (5% nitric acid, 95% ethanol) to reveal the matrix structure. Microstructural identification, shape classification and terminology have been carried out according to standard UNE-EN ISO 945-1.

The X-ray diffraction (XRD) equipment used to characterize the crystal structures of the alloys was a model D8 ADVANCE (BRUKER, Karlsruhe, Germany), with Cu Kα radiation, operated at 40 kV and 30 mA. The diffraction diagrams were measured at the diffraction angle 2θ, range from 10° to 90° with a step size of 0.05°, and 5 s/step. The powder diffraction file (PDF) database 2008 was applied for phase identification. The microstructure, the different regions and the averaged overall chemical composition of each sample were investigated by an optic microscope model DMI5000 M (LEICA Microsystems, Wetzlar, Germany) and a scanning electron microscope (SEM), equipped with an energy-dispersive X-ray spectrometry (EDS) model JSM-5910LV (JEOL, Croissy-sur-Seine, France). The quantitative analysis of volume fractions of different phases was performed for each chemical composition and the average values were calculated using image analysis software.

2.4. Mechanical Characterization

Vickers hardness FM-700 model (FUTURE-TECH, Kawasaki, Japan) was employed on the polished sample surface using a 10 kg load, applied for 10 s. At least five random individual measurements were made.

3. Results and Discussion

3.1. Thermodynamic Equilibrium Phase Diagram of the Alloys

In Figure 1 the equilibrium phase diagram of the elemental composition (Table 1) of the alloy with a variable Al content is plotted. For the sake of simplicity of the diagram, only the principal elements (Fe-C-Si-Mn-Al) were taken in account in the thermodynamic calculations. The as-cast microstructures of each alloy subsequently observed by OM were correlated with the mass percent of Al in the diagram. The microstructural evolution of the samples with 0 wt. % (0-Al), 2 wt. % (2-Al), 7 wt. %. (7-Al) and 15 wt. %. (15-Al) of Al are further discussed in the following section.

As can be seen in Figure 1, the thermodynamic calculations suggested that the phase diagram can be roughly classified in four different regions in function of the wt. % of Al and the stable phases. Firstly, in the region (Region A, highlighted in green) with the lowest wt. % of Al (from 0~6 wt. % Al), the major stable phases are FCC (austenitic matrix), BCC (ferritic matrix), graphite and M_7C_3 carbides. The M_7C_3 carbide phase is only stable at temperatures below 381 °C.

The line designated as "Kappa line" (dark blue line), separates Region A (FCC, BCC, graphite and M_7C_3) and Region B (highlighted in blue). In Region B (between ~6 wt. % and ~9 wt. % Al), the kappa-carbide phase is in thermodynamic equilibrium. The kappa phase was thermodynamically described in Al-C-Fe system [27], and was considered as a high-temperature phase in Fe-C-Al alloys [28].

BCC, graphite and M_7C_3 phases. The major subregion in this range indicates the stabilization of BCC + graphite + kappa over wide range of temperatures and up to 15 wt. % of Al, especially at high temperatures.

Then, in the range from ~9 wt. % to ~13 wt. % Al (Region C, highlighted in yellow) there is a significant qualitative change in the stable phases in the diagram. This region is distinguished from Region 2 by a light brown line. When the amount of Al is over 9.4 wt. %, and at temperatures below 730 °C graphite is not in thermodynamic equilibrium. There are two different subregions, the stable phases are BCC + kappa and BCC + kappa + M_7C_3 (up to ~11.2 wt. % Al), respectively.

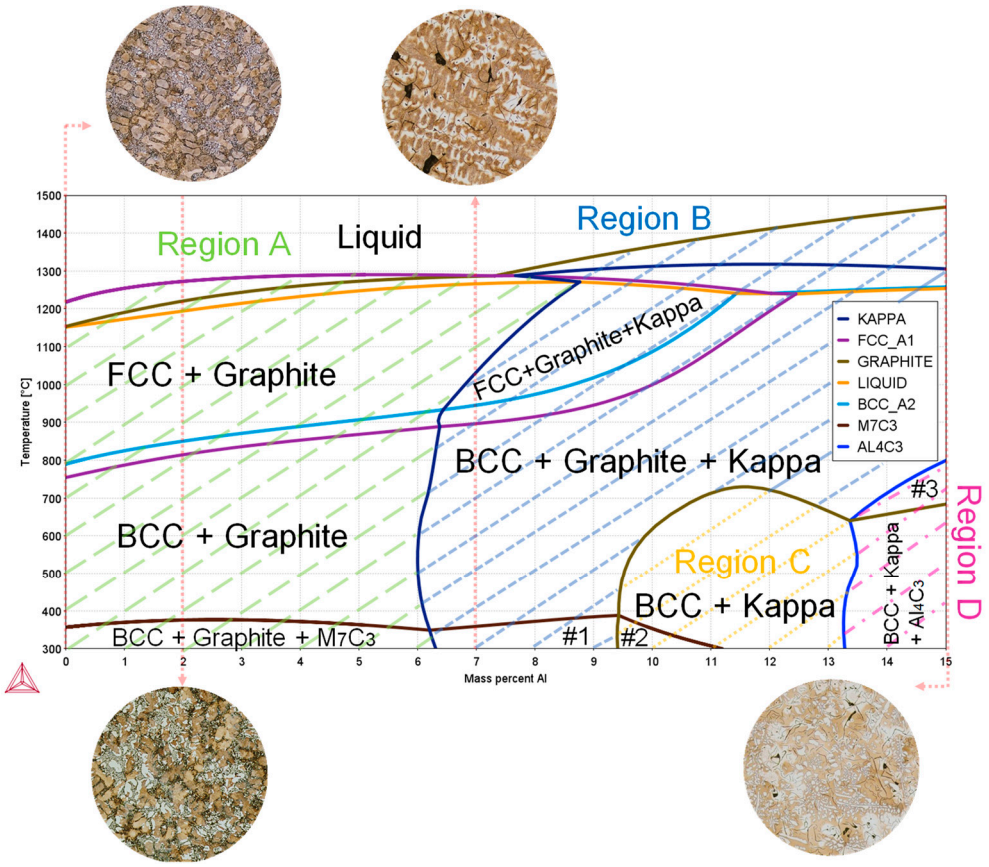

Figure 1. Phase diagram of the nominal composition of the Fe-3.1C-2.0Si-0.6Mn alloy with variable wt.% of Al correlated with the etched microstructures subsequently observed by OM (#1 = BCC + Graphite + kappa + M_7C_3; #2 = BCC + kappa + M_7C_3; #3 = BCC + kappa + M_7C_3 + Al_4C_3).

Finally, in Region D (highlighted in pink) in the range between 13–15 wt. % Al (delimited by the bright blue line), there are two different subregions. In the first one (denoted as #3 in the diagram), above 13.4 wt. % Al and between 632~800 °C, the stable phases are BCC + kappa + Al_4C_3. In the second one, above 13.4 wt. % Al and below 632 °C the stable phases are BCC + kappa + Al_4C_3. Therefore, when the amount of Al is over ~13 wt. %, Al_4C_3 carbides also are stabilized at temperatures below ~800 °C.

Therefore, from the thermodynamic calculations, graphite is not expected to be in thermodynamic equilibrium in Region C and Region D. In addition, increasing the Al content promotes the formation of M_7C_3, kappa and Al_4C_3 phases.

Since the alloys were thermodynamically modelled with the goal of the development of novel lightweight materials, the densities at room temperature of the selected alloys were calculated by Thermo-Calc. The calculated densities are from 7.22 g/cm^3 (Al-free alloy, 0-Al) to 6.05 g/cm^3 for the alloy containing 15 wt. % Al (15-Al). The densities of the alloys are further discussed in Section 3.4 (Hardness of the Samples).

3.2. Alloy Composition and Microstructure of the Cast Samples

The chemical composition of the studied cast irons obtained by ICP is summarized in Table 2. The result obtained by OES (Table 1) and ICP in 0-Al alloy shows good agreement.

Table 2. Elemental composition of Al-alloyed cast irons in wt. % obtained by ICP.

Alloy	Fe	C	Al	Si *	Mn	P	S	Cr	Ni	Mo	Cu
0-Al	Bal.	3.19	0.01	2.53	0.65	0.02	0.02	0.15	<0.10	<0.10	0.10
2-Al	Bal.	3.04	1.80	2.83	0.66	0.02	0.02	0.18	<0.10	<0.10	0.10
7-Al	Bal.	2.85	7.30	2.74	0.62	0.02	0.02	0.16	<0.10	<0.10	0.09

15-Al	Bal.	2.65	15.0	2.33	0.55	0.02	0.02	0.16	<0.10	<0.10	0.09

* The content of Si was estimated by SEM + EDS.

The XRD patterns in Figure 2 showed the formation of graphite and BCC phases in 0-Al and 2-Al cast irons, which demonstrates good agreement with CALPHAD (CALculation of PHAse Diagrams) in Figure 1. On the other hand, the XRD peaks of the 7-Al alloy indicates the stabilization of BCC, graphite and kappa-carbides ($AlFe_3C_{0.5}$) as a function of increasing aluminum content. The indexed phases showed good agreement with the major subregion (BCC + graphite + kappa) in Region B obtained by CALPHAD calculations. Finally, in 15-Al cast iron, the peaks corresponding to kappa carbides, graphite and BCC phases also were indexed. The indexed peaks also showed good agreement with the major subregion in Region B.

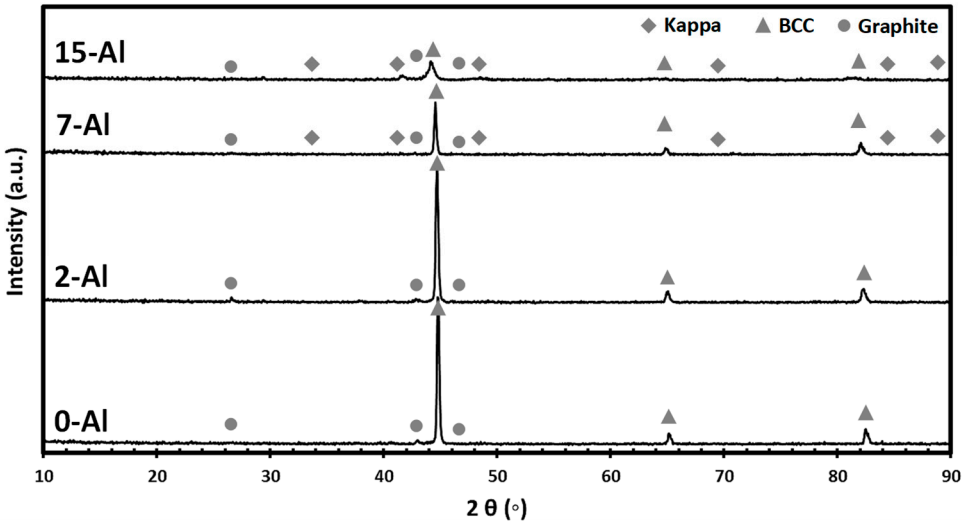

Figure 2. X-ray diffraction (XRD) patterns of the developed cast irons.

In Figure 3 the etched OM (a, d, g and j) and SEM images for each of the studies alloys are shown. Images confirmed the formation of two phases. Thus, the microstructure of 0-Al alloy in Figure 3a–c displays a "D" type morphology that indicates an overcooled graphite. The fine graphite flakes are uniformly distributed in a pearlitic matrix, and a low fraction of ferrite.

In Figure 3d–f the microstructure of 2-Al cast iron shows a "D"/"E" type distribution that indicate an overcooled graphite and low carbon equivalent. The alloy also displays a pearlitic microstructure with some ferrite, which agrees with the results obtained by XRD.

In Figure 3j–l, the microstructure of 7-Al displays ferritic matrix with dispersed perlite. The graphite flakes show a large morphology that indicates the presence of primary graphite. The microstructure also shows a "D"/"E" type distribution that indicate an overcooled graphite and low carbon equivalent. The microstructure also shows the stabilization of kappa carbides, demonstrating good agreement with the results obtained by XRD.

Finally, in Figure 3j–l the microstructure of 15-Al shows similar pattern to alloy containing 7 wt. %. Al, but the graphite shows coarser morphology.

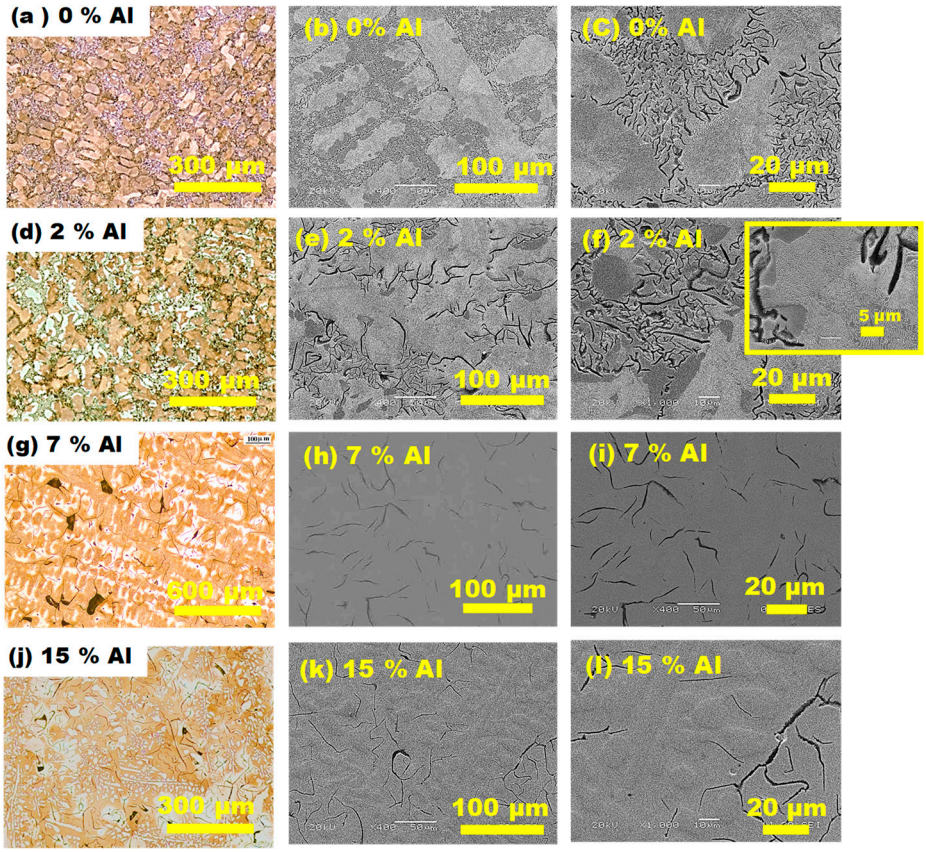

Figure 3. (**a**–**c**) Etched optical microscopy (OM) and SEM images of 0-Al; (**d**–**f**) etched OM and SEM images of 2-Al; (**g**–**i**); etched OM and SEM images of 7-Al and (**j**–**l**) etched OM and SEM images of 15-Al.

To determine the effect of Al on the graphite morphology of the cast iron, the non-etched OM of the alloys are shown in Figure 4. The microstructures show that the perlite content decrease with the increment of wt. % of Al. The opposite occurs with the ferrite.

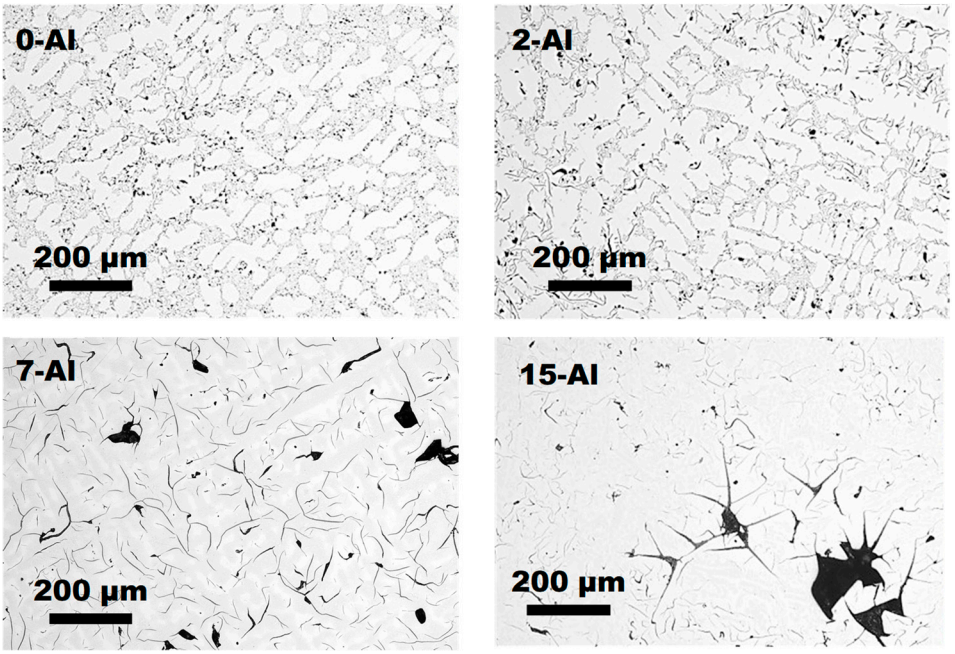

Figure 4. Effect of Al on the graphite morphology in the microstructure of alloys containing 0 wt.%, 2 wt.%, 7 wt.% and 15 wt.% Al.

In the case of graphite, a slight increment occurs with 2 wt. % of Al, but a great decrease occurs until 15 wt. % of Al. This indicates that Al in low quantity is a graphite stabilizer. On the other hand, as the quantity of Al increases, it becomes a carbide former with a subsequent reduction in the amount of graphite.

The quantitative results of the volume fraction of the characterized phases of the studied alloys obtained by image analysis are summarized in Table 3. The analysis of ferrite volume fraction for 7-Al and 15-Al are not only for ferrite. Due to the uncertainty of the method to distinguish between both phases, ferrite and kappa-carbides are quantified together.

Table 3. Phase volume fraction of the studied alloys.

Alloy	Ferrite (%)	Graphite (%)	Perlite (%)
0-Al	9.2	8.1	82.7
2-Al	15.5	8.6	75.9
7-Al	26.9 *	7.1	66.0
15-Al	36.1 *	5.5	56.8

* Ferrite + kappa-carbides.

3.3. Analysis of the Cooling Curves

The solidification properties of the studied cast irons were obtained by TA of the solidification curves and its derivatives. In Figure 5 the cooling curves of the studied cast irons are shown. For the sake of simplicity, only the solidification curves are plotted.

As can be seen from the solidification curves, the solidification changes from a completely hypoeutectic to a relative eutectic behavior, with a recalescence that remains stable at the eutectic temperature for nearly 26 s in the alloy containing 15 wt. % of Al. In the alloy containing 7 wt. % Al no recalescence is observed, and the temperature does not stop falling at any time, indicating low graphitic precipitation.

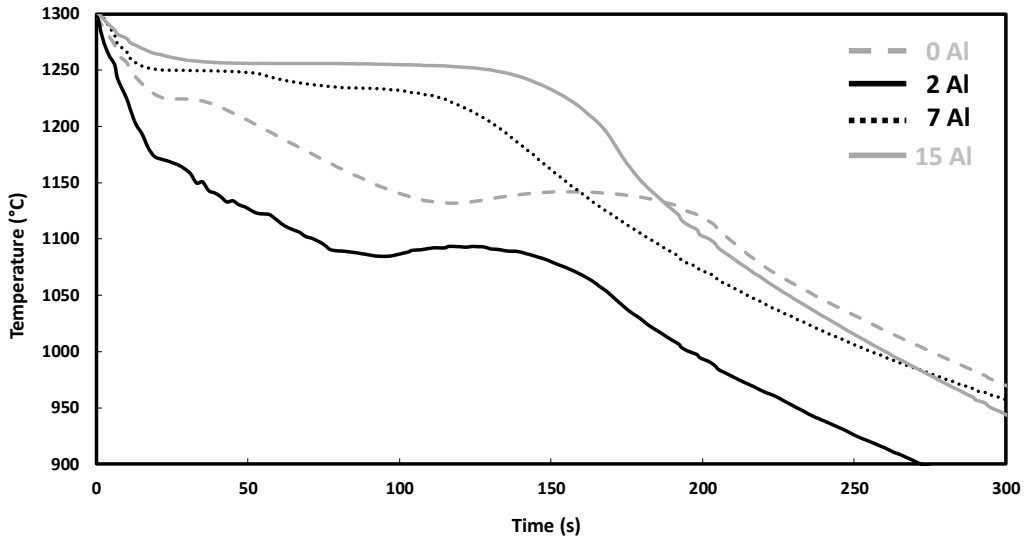

Figure 5. The cooling curves of the studied cast irons.

In conventional TA of standard grade cast irons there are two important points in the interpretation of the cooling curves, known as low and high eutectic points. These points also are known as eutectic undercooling and eutectic recalescence, respectively. From these points, characteristics of the free graphite forming can be defined, as well as important aspects of the quality of the cast irons. The recalescence parameter is known as the difference between both eutectic points and is assessed as one of the key parameters of the metallurgical quality of the cast irons.

Even though in Fe-Al system there is no similar eutectic point for the studied alloys (at 7 wt. %. Al a similar region can be identified, but with different definition and geometry from one of the cast irons), the cooling curves show similar evolution than standard cast iron ones, probably due to the Fe–C relation.

To analyze the cooling curves obtained in this work, these points with similarities with conventional low and high eutectic points have been defined as eutectic undercooling and eutectic recalescence points. Finally, the recalescence was defined as the difference between them. Therefore, the aforementioned points, the liquidus temperature (T_{liq}) and solidus temperature (T_{sol}) are shown in Table 4.

Table 4. Solidification properties of the cooling curves.

Alloy	Liquidus (°C)	Solidus (°C)	Eutectic Undercooling (°C)	Eutectic Recalescence (°C)	Recalescence Time (s)	
0-Al	1224	1082	1132	1142	10	39
2-Al	1168	1044	1084	1093	9	29
7-Al	1250	1170	--	--	--	--
15-Al	1264	1179	1256	1256	0	26

3.4. Hardness of the Samples

The bulk hardness of the studied alloys was studied on Vickers hardness tester under the load of 10 kg. The mean values with the standard deviation are summarized in Table 5. The addition of Al increases the hardness of the alloys, but not gradually, as the alloy with the highest hardness is 7-Al. This is correlated with the formation of kappa phase and finer perlite.

Table 5. Hardness, calculated density and specific hardness of the studied cast irons.

Alloy	Hardness (HV 10)	Density (g/cm^3)	Specific Hardness (HV/g·cm^{-3})
0-Al	235 ± 14	7.22	32.5
2-Al	251 ± 15	7.04	35.6
7-Al	363 ± 06	6.62	54.8
15-Al	334 ± 25	6.05	55.2

Since the alloys were designed with the goal of the development of novel lightweight materials, the densities at room temperature of the developed alloys also were calculated by Thermo-Calc in Table 5. The densities are between 7.22 g/cm^3 (0-Al) and 6.05 g/cm^3 for the alloy containing 15 wt. % Al (15-Al). Furthermore, the specific hardness of 15-Al cast iron is the highest of the results obtained. This is due to a combination of low density and high hardness of the alloy.

A comparison of the hardness and calculated density at room temperature of the developed cast irons with related works in the field [18,20,21,25] is given in Figure 6. As can be seen, the 0-Al cast iron showed a density of 7.22 g/cm^3 and a hardness value of 235 ± 14 HV 10, which is in accordance with the typical range between 186–247 HV of the EN-GJL-HB195 grade cast iron. The developed alloys showed good agreement in terms of hardness and density with previously published works. It should be noted that 15-Al cast iron shows quite similar properties to Fe-3.0C-16.0Al-2.2Si cast iron [18].

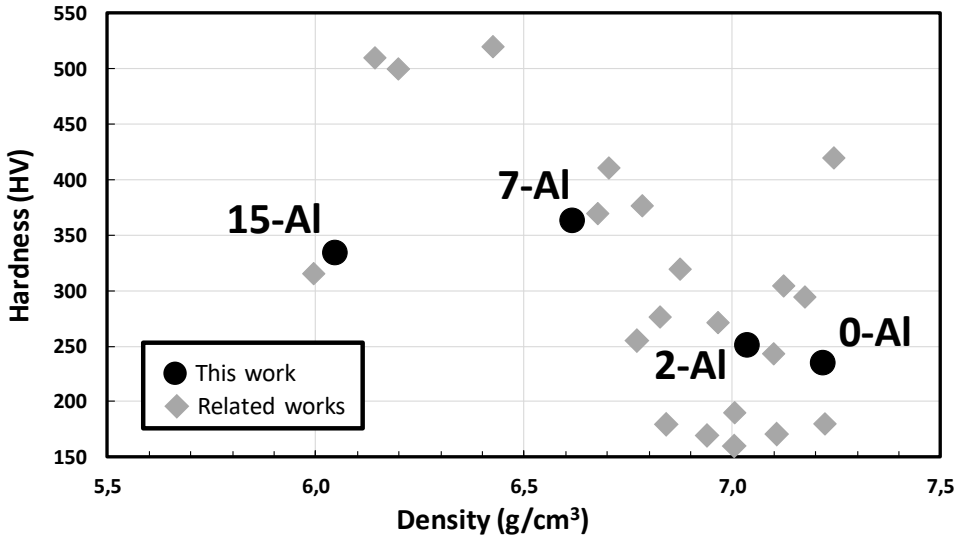

Figure 6. Materials property space for hardness vs. calculated density at room temperature of manufactured cast irons and related works, data from [18,20,21,25].

4. Conclusions

In this work, the microstructural evolution and hardness of four lightweight cast irons as a function of increasing aluminum content (from 0 wt. % to 15 wt. %) was studied. The alloys were manufactured by an easily scalable and affordable gravity casting process. The following conclusions were obtained:

- The phase diagram of the alloys in function of the wt. % of Al can be divided in four regions in function of the stable phases. From the phase diagram, graphite is not expected to be in thermodynamic equilibrium over 9,4 wt. % Al at low temperatures (Region C and D). But the observed microstructures showed the formation of graphite, which means that thermodynamic equilibrium of 15-Al is over ~800 °C (Region B).
- From thermodynamic calculations, the increasing of the Al content also promotes the formation of M_7C_3, kappa-carbides and Al_4C_3 phases. Al_4C_3 carbides are in thermodynamic equilibrium when the amount of Al is over ~13 wt. %. Therefore, according to thermodynamic calculations, there is a limit as to where, in addition to Al_4C_3 phase, kappa-carbides are also stabilized.
- The microstructure of 0-Al alloy is formed by a fine graphite flakes distributed in a pearlitic matrix, and a low fraction of ferrite. The microstructure of 2-Al alloy also shows a pearlitic matrix with ferrite, but "D"/"E" type distribution with overcooled graphite. The microstructure of 7-Al alloy is formed by a ferritic matrix with dispersed perlite. The graphite flakes show a large morphology that indicates the presence of primary graphite. The microstructure also shows the stabilization of kappa-carbides. The microstructure of 15-Al graphite shows a similar pattern to alloy containing 7 wt. %. Al, but the graphite shows coarser morphology.
- The microstructures show that the perlite content decrease with the increment of wt. % of Al. The opposite occurs with the ferrite. In the case of graphite, a slight increment occurs with 2 wt. % of Al, but a great decrease occurs until 15 wt. % of Al.
- The cooling curves of the studied cast irons shows that recalescence is not observed in 7-Al cast iron. The solidification changes from a hypoeutectic to a eutectic behavior, with a recalescence that remains stable at the eutectic temperature in 15-Al cast iron.
- The addition of Al increases the hardness of the studied cast irons, but not gradually. The alloy with the highest hardness is 7-Al, which is correlated with the formation of kappa carbides and finer perlite.

- The obtained properties showed good consistency in terms of hardness vs. density with related works in the field.

As a future work, based on the obtained results, it is suggested the manufacturing of alloys containing 7 wt. % and 15 wt. % or more Al, to further study the mechanical properties. Specifically, it can be interesting the intensive study of the tribological properties of high Al-alloyed (≥7 wt. % Al) cast irons.

Author Contributions: Conceptualization, J.M.S.; Formal analysis, A.O.; Funding acquisition, D.E.; Investigation, J.M.S., J.C.G., G.A. and I.H.; Methodology, A.O.; Project administration, I.Q.; Resources, P.R.; Supervision, D.E., J.C.G., G.A., I.H., I.Q. and P.R.; Validation, D.E. and J.C.G.; Writing—original draft, J.M.S.; Writing—review and editing, J.M.S. All authors have read and agreed to the published version of the manuscript.

Funding: This work has been partially funded by the Basque Government through the project Elkartek LION: KK-2019/00040.

Conflicts of Interest: The authors declare no conflict of interest.

References

1. Mitrica, D.; Badea, I.C.; Olaru, M.T.; Serban, B.A.; Vonica, D.; Burada, M.; Geanta, V.; Rotariu, A.N.; Stoiciu, F.; Badilita, V.; Licu, L. Modeling and experimental results of selected lightweight complex concentrated alloys, before and after heat treatment. *Materials* **2020**, *13*, 4330, doi:10.3390/ma13194330.
2. Tun, K.S.; Charadva, V.; Gupta, M. Lightweight medium entropy magnesium alloy with exceptional compressive strength and ductility combination. *J. Mater. Eng. Perform.* **2021**, *30*, 2422–2432, doi:10.1007/s11665-021-05478-w.
3. Chandel, R.; Sharma, N.; Bansal, S.A. A review on recent developments of aluminum-based hybrid composites for automotive applications. *Emergent Mater.* **2021**, 1–15, doi:10.1007/s42247-021-00186-6.
4. Wallerstein, D.; Salminen, A.; Lusquiños, F.; Comesaña, R.; García, J.D.V.; Rodríguez, A.R.; Badaoui, A.; Pou, J. Recent developments in laser welding of aluminum alloys to steel. *Metals* **2021**, *11*, 1–32, doi:10.3390/met11040622.
5. Zhou, B.; Liu, B.; Zhang, S. The advancement of 7xxx series aluminum alloys for aircraft structures: A review. *Metals* **2021**, *11*, 718, doi:10.3390/met11050718.
6. Kaltzakorta, I.; Gutierrez, T.; Elvira, R.; Jimbert, P. Manufacturing and forging issues encountered while upscaling 1.3C30Mn10Al-austenitic and 0.65C12Mn-duplex low-density steels. *Mater. Manuf. Process.* **2021**, *00*, 1–12, doi:10.1080/10426914.2021.1944192.
7. Moon, J.; Ha, H.Y.; Kim, K.W.; Park, S.J.; Lee, T.H.; Kim, S.D.; Jang, J.H.; Jo, H.H.; Hong, H.U.; Lee, B.H.; et al. A new class of lightweight, stainless steels with ultra-high strength and large ductility. *Sci. Rep.* **2020**, *10*, 1–10, doi:10.1038/s41598-020-69177-7.
8. Liu, D.; Ding, H.; Han, D.; Cai, M.; Lee, Y.K. Microstructural evolution and tensile properties of Fe–11Mn–10Al-1.2C medium-Mn lightweight steel. *Mater. Sci. Eng. A* **2020**, *797*, 140256, doi:10.1016/j.msea.2020.140256.
9. Wang, Z.; Lu, W.; Zhao, H.; He, J.; Wang, K.; Zhou, B.; Ponge, D.; Raabe, D.; Li, Z. Formation mechanism of κ-carbides and deformation behavior in Si-alloyed FeMnAlC lightweight steels. *Acta Mater.* **2020**, *198*, 258–270, doi:10.1016/j.actamat.2020.08.003.
10. Kaltzakorta, I.; Gutiérrez, T.; Elvira, R.; Guraya, T.; Jimbert, P. Low density steels for forging. *Mater. Sci. Forum* **2018**, *941*, 287–291, doi:10.4028/www.scientific.net/MSF.941.287.
11. Chen, S.; Rana, R.; Haldar, A.; Ray, R.K. Current state of Fe-Mn-Al-C low density steels. *Prog. Mater. Sci.* **2017**, *89*, 345–391.
12. Kaltzakorta, I.; Gutierrez, T.; Elvira, R.; Jimbert, P.; Guraya, T. Evolution of microstructure during isothermal treatments of a duplex-austenitic 0.66C11.4Mn.9.9Al low-density forging steel and effect on the mechanical properties. *Metals* ***2021***, *11*, 214, doi:10.3390/met11020214.
13. Pero-Sanz Elorz, J.A.; Fernández González, D.; Verdeja González, L.F. *Physical Metallurgy of Cast Irons*; Springer: Cham, Switzerland, 2018.
14. Verhoeven, J.D. Cast Irons. In *Steel Metallurgy for the Non-Metallurgist*; ASM International: Novelty, OH, USA, 2019.
15. Davis, J.R. (Ed.) *ASM Specialty Handbook: Cast Irons*; ASM International: Materials Park, OH, USA, 1996.
16. Bourdie, J.; Bruneseaux, F.; De Parseval, P.; Gouy, S.; Laffont, L.; Lacaze, J. Effect of cooling rate and aluminium addition on graphite growth during solidification and graphitization. *Mater. Sci. Forum* **2018**, *925*, 20–27, doi:10.4028/www.scientific.net/MSF.925.20.
17. Haque, M.M.; Young, J.M. Production of spheroidal graphite aluminium cast iron and the factors affecting it. *J. Mater. Process. Technol.* **1995**, *55*, 186–192, doi:10.1016/0924-0136(95)01952-9.
18. Ibrahim, M.M.; Mourad, M.M.; Nofal, A.A.; Farahat, A.I.Z. Microstructure, hot oxidation resistance and damping capacity of Al- alloyed cast iron. *Int. J. Cast Met. Res.* **2017**, *30*, 61–69, doi:10.1080/13640461.2016.1239895.

19. Gumienny, G.; Kurowska, B.; Klimek, L. Aluminium in compacted graphite iron. *China Foundry* **2020**, *17*, 137–143, doi:10.1007/s41230-020-9013-x.
20. Shayesteh-Zeraati, A.; Naser-Zoshki, H.; Kiani-Rashid, A.R. Microstructural and mechanical properties (hardness) investigations of Al-alloyed ductile cast iron. *J. Alloys Compd.* **2010**, *500*, 129–133, doi:10.1016/j.jallcom.2010.04.003.
21. Aguado, E.; Ferrer, M.; Larrañaga, P.; Stefanescu, D.M.; Suárez, R. The effect of the substitution of silicon by aluminum on the properties of lamellar graphite iron. *Int. J. Met.* **2019**, *13*, 536–545, doi:10.1007/s40962-018-00303-y.
22. Kasvayee, K.A.; Ghassemali, E.; Svensson, I.L.; Olofsson, J.; Jarfors, A.E.W. Characterization and modeling of the mechanical behavior of high silicon ductile iron. *Mater. Sci. Eng. A* **2017**, *708*, 159–170, doi:10.1016/j.msea.2017.09.115.
23. Takamori, S.; Osawa, Y.; Halada, K. Aluminum-alloyed cast iron as a versatile alloy. *Mater. Trans.* **2002**, *43*, 311–314, doi:10.2320/matertrans.43.311.
24. Adebayo, A.O.; Oyetunji, A.; Alaneme, K.K. Microstructural characteristics, mechanical and wear behaviour of aluminium-alloyed ductile irons subjected to two austempering processes. *Acta Polytech.* **2020**, *60*, 185–196, doi:10.14311/AP.2020.60.0185.
25. Sandikoglu, A.; Gecu, R. Microstructural, mechanical and tribological characterization of aluminum-alloyed ductile cast irons based on aluminum content. *J. Alloys Compd.* **2021**, *879*, 160428, doi:10.1016/j.jallcom.2021.160428.
26. Andersson, J.O.; Helander, T.; Höglund, L.; Shi, P.; Sundman, B. Thermo-Calc & DICTRA, computational tools for materials science. *Calphad Comput. Coupling Phase Diagrams Thermochem.* **2002**, *26*, 273–312, doi:10.1016/S0364-5916(02)00037-8.
27. Zheng, W.; He, S.; Selleby, M.; He, Y.; Li, L.; Lu, X.G.; Ågren, J. Thermodynamic assessment of the Al-C-Fe system. *Calphad* **2017**, *58*, 34–49, doi:10.1016/j.calphad.2017.05.003.
28. Cheng, W.C.; Song, Y.S.; Lin, Y.S.; Chen, K.F.; Pistorius, P.C. On the eutectoid reaction in a quaternary Fe-C-Mn-Al alloy: Austenite → ferrite + kappa-carbide + M23C6 carbide. *Metall. Mater. Trans. A Phys. Metall. Mater. Sci.* **2014**, *45*, 1199–1216, doi:10.1007/s11661-013-2083-2.